DEUTSCHES ELEKTRONEN – SYNCHROTRON

DESY 90-160
FTUAM-EP-90-04
December 1990

Gluon Extraction from Charm and Bottom Production at LEP/LHC

K.J. Abraham
Nikhef-H, Amsterdam, The Netherlands

H. Jung
III. Phys. Institut, Lehrstuhl B, RWTH Aachen

G. A. Schuler
II. Institut für Theoretische Physik, Universität Hamburg

J.F. de Trocóniz
Universidad Autónoma de Madrid, Spain

ISSN 0418-9833

NOTKESTRASSE 85 · D-2000 HAMBURG 52

To be sure that your preprints are promptly included in the HIGH ENERGY PHYSICS INDEX , send them to the following address (if possible by air mail) :

DESY
Bibliothek
Notkestrasse 85
2 Hamburg 52
Germany

DESY 90–160
FTUAM-EP-90-04
December 1990

ISSN 0418–9833

Gluon Extraction from Charm and Bottom Production at LEP/LHC[1]

K. J. Abraham[a], H. Jung[b], G. A. Schuler[c], J. F. de Trocóniz[d2],

[a] *Nikhef-H, Amsterdam, The Netherlands*

[b] *III. Phys. Institut, Lehrstuhl B, RWTH Aachen, FRG*

[c] *II. Institut für Theoretische Physik [3], Universität Hamburg, FRG*

[d] *Dpto. de Física Teórica, Universidad Autónoma de Madrid, Spain*

Abstract

We discuss heavy quark production in ep collisions at LEP/LHC energies. The various production mechanisms as well as background processes are studied. We succeed in separating the direct photon-gluon fusion channel, and show how to measure the gluon density in both open and hidden heavy quark production at LEP/LHC. We specify the explorable ranges in x and Q^2 and estimate the errors with which the gluon density may be reconstructed at LEP/LHC.

[1] To be published in the Proceedings of the ECFA Workshop on LHC, Aachen, FRG (1990).
[2] Partially supported by the exchange programme CICYT-Kfz., Karlsruhe.
[3] Supported by Bundesministerium für Forschung und Technologie, 05 4HH 92P/3, Bonn, FRG.

1 Introduction

The primary source of information on parton distributions comes from structure functions measured in deep inelastic scattering experiments. Taking appropriate combinations of charged current and neutral current events, combining e^+p and e^-p data, and choosing suitable kinematic ranges, it is possible to unfold individual quark distributions at LEP/LHC[1]. Inclusive lepton scattering, however, is not directly sensitive to the gluon distribution. A dependence on the glue (simultaneously with a dependence on Λ) arises through the Q^2 evolution of (singlet) structure functions or through contributions from the longitudinal structure function $F_L(x,Q^2)$ (see [2,3] for corresponding studies at LEP/LHC). In this note we investigate the prospects of determining the gluon density from exclusive processes, namely open and hidden heavy flavour production. Previous attempts to extract the gluon distribution from heavy quark production can be found in [4,5]. The new methods we develop in this first systematic study could also be used at the HERA experiments.

At ep colliders, heavy quarks are mainly produced via exchange of quasi-real photons ($Q^2 \approx 0$). The scattered electron is typically lost into the beam pipe. Heavy quark production at ep colliders can thus be viewed as a continuation of photoproduction experiments up to higher cms energies. The leading order production mechanism of heavy quarks is photon gluon fusion

$$\gamma + g \;\rightarrow\; c + \bar{c}\,,\; b + \bar{b} \qquad (1)$$

$$\gamma + g \;\rightarrow\; J/\Psi + g\,. \qquad (2)$$

For the following reasons heavy quark production looks well suited for a measurement of the gluon density: (i) the direct sensitivity to the gluon density, (ii) the comfortable rates, and (iii) the clean signatures.

Cross section estimates for (1,2) depend rather heavily on the values of the mass scales in the strong coupling constant α_s and the gluon density. In contrast to lepton inclusive ep scattering the scale μ in (1,2) is not uniquely defined. According to QCD factorization μ has to be of order of the heavy quark mass. We identify mass and renomalization scales and take $\mu = \sqrt{\hat{s}}$, the partonic cms energy. Furthermore we use throughout this paper the one-loop formula for α_s with four flavours and take $\Lambda_{QCD} = 200\,\mathrm{MeV}$. If not otherwise stated the parton density parametrization set B1 of Morfin and Tung[6] is used.

The rather strong dependence on the choice of the scale indicates that higher order corrections are important. For open heavy flavour production these corrections can be calculated perturbatively. Since we shall require a substantial invariant mass for the heavy quark pair in our analysis, corrections from quark initiated subprocesses, $\gamma + q \rightarrow q + g(\rightarrow Q\bar{Q})$, will be greatly reduced. But the remaining corrections are gluon initiated, exactly as the leading contribution (1). Furthermore it is expected that these corrections can be described by a rather constant K-factor[7]. Thus we generate events according to (1) and assume $K(c\bar{c}) = K(b\bar{b}) = 2$. We do, however, include effects of multiple gluon emission on the event topology by using the event generator AROMA[8] where they are

included in a parton cascade approach. Higher order corrections to J/Ψ production are more difficult to estimate since the calculations assume the validity of the non relativistic quarkonium model. In [9] it was shown that this model describes differential distributions well, if $z < 0.8$ and $p_T > 1\,\mathrm{GeV}$. We shall therefore apply these cuts later when reconstructing the quantities z and p_T. However, there is a problem with absolute normalisation, a K-factor of about two seems to be required to fit the data. For simplicity we take K=1.

2 J/Ψ analysis

The subprocesses contributing to J/Ψ production in addition to (2) are:

$$\gamma + g \;\rightarrow\; b\,(\rightarrow \Psi X) + \bar{b} \qquad (3)$$

$$g + g \;\rightarrow\; \chi \rightarrow \Psi + \gamma \qquad (4)$$

and

$$\begin{aligned} g + g &\rightarrow \Psi + g \qquad (5)\\ \{gg, q\bar{q}\} &\rightarrow \chi\,(\rightarrow \Psi + \gamma) + g\\ gq &\rightarrow \chi\,(\rightarrow \Psi + \gamma) + q\,. \end{aligned}$$

Additional background events may come from the production of light quark events with subsequent decays into leptons. Our analysis is based on the leptonic decay, $J/\Psi \rightarrow l^+l^-$, where l is either an electron or a muon. By restricting the lepton invariant mass to the J/Ψ mass these background events can be rejected. We thus do not consider these events any further. Corrections given by the hadronic component of the photon (4,5) are known to be large[10]. These resolved photon contributions give rise to $q\bar{q}$, qg, gq, and gg initial states. A K-factor of about two is required in the analyses of J/Ψ production at the SPS and the Tevatron where at high enough energies the dominant contributions come from gluon-gluon fusion to χ states [11,12]. Assuming that the K-factors for (4,5) will be similar, the K-factors for the resolved and direct processes will be roughly the same. Hence we use uncorrected Born level cross sections (K=1 also for (4,5)) in order to optimise cuts.

The p_T distributions of the various J/Ψ production mechanisms are shown in fig. 1 with the labels: solid line: direct production (2), dashed line: resolved photon contributions (5), and dashed-dotted line: b-decays (3). The curves show the Monte Carlo p_T^Ψ distributions where no cut was applied. The subprocess (4) can only produce J/Ψ's with small transverse momentum and is therefore omitted. At high p_T values ($p_T \gtrsim 5\,\mathrm{GeV}$) the bottom production mechanism (3) dominates. Yet, for $p_T \lesssim 4\,\mathrm{GeV}$ it can safely be neglected. J/Ψ's from b-decays could further be reduced by requiring them to be isolated. The other two processes, (2) and (5), are about equally large. They have similar p_T distributions and can thus not be discriminated by a cut in p_T.

Direct photon (2) and resolved photon (5) contributions do, however, differ in the laboratory polar angle distribution of the J/Ψ. In fig. 2 we show $d\sigma/d\cos\theta$

for both subprocesses. Again, the distributions are Monte Carlo results without applying any cut except $p_T > 1\,\mathrm{GeV}$. We find a rather flat distribution for the direct process whereas the resolved photon process is strongly peaked at $\cos\theta \equiv (\vec{p}_\Psi \cdot \vec{p}_p)/(|\vec{p}_\Psi| \cdot |\vec{p}_p|) = 1$, i.e., in the direction of the outgoing proton remnant [4]. A cut in $\cos\theta$ will therefore be very effective in suppressing the latter reaction.

For our analysis we now generate complete event samples for both processes. The hadronization is implemented using the LUND string fragmentation. The events are then passed through a detector of H1 type[13]. The J/Ψ momenta are reconstructed in the tracking system via their decay leptons. Due to the geometrical acceptance this implies a cut of $|\cos\theta| < 0.98$ on the (reconstructed) polar angle. Referring to fig. 2 it is clear that this diminishes the resolved photon contribution quite a lot compared to the "signal events" (2). We now apply a cut on the transverse J/Ψ momentum, $p_T^\Psi > 1\,\mathrm{GeV}$, in order to select events where (2) is a reliable description of J/Ψ production. After the two requirements, (i) the J/Ψ's can be reconstructed in the tracking device, and (ii) $p_T^\Psi > 1\,\mathrm{GeV}$, we find a signal-to-background ratio $S/B \approx 5$, i.e. the direct contribution (2) is approximately a factor five larger than the resolved one (5).

In order to improve the signal to background ratio we consider the distribution in z: the ratio of energie-plus-longitudinal-momentum of the J/Ψ to the photon in the laboratory frame:

$$z = \frac{p_p \cdot p_\Psi}{p_p \cdot p_\gamma} \underbrace{=}_{\mathrm{Lab}} \frac{(E + p_L)_\Psi}{(E + p_L)_\gamma}\,. \qquad (6)$$

The momenta are labelled as proton p_p, photon p_γ, and J/Ψ p_Ψ. As argued in ref.[14], J/Ψ's carry almost all of the incident energy when the proton and photon couple directly but only a small fraction when they couple indirectly, i.e. via the partons in the photon. This is a consequence of the soft parton distribution in the photon. This is quantified in fig. 3 where we show the z-distributions of the two processes as they are obtained from the Monte Carlo. The direct channel peaks at $z \rightarrow 1$, whereas the resolved photon contributions accumulate near $z = 0$. A cut in z will therefore substantially improve S/B provided z can well be reconstructed.

Experimentally, z in (6) has to be reconstructed from a measurement of the momentum of the exchanged photon. The photon momentum is determined by the variable y defined by

$$y = \frac{p_p \cdot p_\gamma}{p_p \cdot p_e} \underbrace{=}_{\mathrm{Lab}} \frac{(E + p_L)_\gamma}{(E + p_L)_e} \qquad (7)$$

where p_e is the incoming electron momentum. As stated above, the exchanged photon is almost real in J/Ψ production. In the collinear approximation, $Q^2 = 0$, we obtain $E_\gamma = (p_L)_\gamma$ or $p_\gamma = y\,p_e$. Independent of this approximation, z is now reconstructed by (neglecting the electron mass):

$$z_{rec} = \frac{(E + p_L)_\Psi}{2\,y_{rec}\,E_e}\,. \qquad (8)$$

[4] Our positive z-axis is defined by the direction of the incoming electron.

We reconstruct y from the calorimeter measurement

$$y_{rec} = \sum_h \frac{(E + p_L)_h}{2E_e} \tag{9}$$

where the sum runs over all particles measured in the calorimeter except the scattered electron[5]. We show in figs. 4a and b the correlation y vs. y_{rec} for J/Ψ production via the direct process (2) and the resolved photon process (5). The reconstructed z distributions can be found in fig. 3 where they are plotted together with the Monte Carlo results. From fig. 4a we find that y can very well be reconstructed over the whole y range using (9) for the direct production channel. Here also the reconstructed z distribution approximates the true (Monte Carlo) distribution very well over the whole z range except near $z = 0$. For J/Ψ's produced via the hadronic component of the photon this method does not work the reason being the spectator jet of the photon. In fact, we have to distinguish the following cases for the resolved photon contributions:

- The photon remnants are fully contained in the calorimter. Then the measurement (9) reconstructs y (7), the energy fraction carried by the photon. Also (8) approximates z as defined in (6). Thus the reconstructed z distribution follows the exact one. This is the region z close to zero in fig. 3.

- The photon remnants are completely lost into the beam pipe. Then (9) gives the energy fraction carried by that parton p^γ within the photon which participated in the hard interaction, $y_{rec} \approx y_p$ with

$$y_p = \frac{(E + p_L)_{p^\gamma}}{2\,E_e} = x_p\, y\,. \tag{10}$$

  Here x_p denotes the momentum fraction of the photon carried by the parton. Since $0 < x_p < 1$ we have $y_{rec} \approx y_p < y$. Consequently a parton-z_p is reconstructed

$$z_p = \frac{p_p \cdot p_\Psi}{p_p \cdot p_{p^\gamma}} \underbrace{=}_{\text{Lab}} \frac{(E + p_L)_\Psi}{(E + p_L)_{p^\gamma}} = \frac{z}{x_p} > z\,. \tag{11}$$

  This creates the peak at $z = 0.9$ in fig. 3 and yields even values $z > 1$. In this case the seen (reconstructed) subprocess is a actually one initiated by a parton inside the *electron* plus a parton inside the proton. If the latter parton is the gluon, then these events are really signal events as (2).

- The photon remnants are only partly be reconstructed. Then (9) yields a value y_{rec} with $y_p < y_{rec} < y$. Correspondingly (8) yields a value z_{rec} with $z < z_{rec} < z_p = z/x_p$. This fills the region $0.2 \lesssim z \lesssim 0.6$ in fig. 3.

Which of the above mentioned situations occurs depends on the acceptance of the calorimeter and the details of the fragmentation of the photon structure function which are far from being understood. In fig. 4b and c we compare for the resolved

[5]We do not include information on the scattered electron energy coming from a luminosity monitor measurement since it is not clear whether the latter will work with the high rates expected at LEP/LHC.

photon contributions y_{rec} versus y and y_p, respectively. It seems that at least in our simulation there is a good correlation between the reconstructed and the partonic y's. Note also, that the photon remnants are usually flying backwards (i.e. keeping the direction of the incoming electron) in contrast to the proton remnants which follow the incoming proton direction.

Despite of the fact that z cannot be reconstructed over its entire region, we apply a cut $z > 0.2$ in order to diminish the resolved photon contributions. Furthermore we require $z < 0.8$ to stay away from elastic and diffractive J/Ψ production. Then we end up with a total J/Ψ cross section of $\sigma(J/\Psi) \times BR(J/\Psi \to l^+l^-) = 0.3\,\text{nb}$. At an integrated luminosity of $1\,\text{fb}^{-1}$ per year this corresponds to about 3×10^5 events. Among these events are then only 13% J/Ψ's coming from resolved photon contributions (5).

We did not attempt to improve further the S/B ratio. In principle one could further discriminate at least against the background from χ production by tagging on the photon in the decay, on the lines of [12]. However, present knowledge of the fragmentation of the spectator jet from the photon is inadequate for the purposes of completely eliminating backgrounds from pion decay.

When trying to measure the gluon density one has to find observables which on the one hand side constraint x_g, the momentum fraction of the proton carried by the gluon, and which, on the other hand, can actually be measured experimentally. We determine x_g from the following relation:

$$x_g = \frac{\hat{s} + Q^2}{y\,s} \tag{12}$$

where $\sqrt{s}$ is the total cms energy and $\sqrt{\hat{s}}$ the partonic cms energy. As mentioned above, the photon virtuality is very small so that we can approximate it by

$$Q^2 \approx Q^2_{rec} = 0\,. \tag{13}$$

The partonic cms energy $\sqrt{\hat{s}}$ can well be measured in J/Ψ events through measurements of $p_T(l\bar{l}) = p_T(\Psi)$ and $z(l\bar{l}) = z(\Psi)$ using the relation

$$p_T^2 = z(1-z)\,\hat{s} - (1-z)\,m_\Psi^2\,. \tag{14}$$

The measurement of y as given in (9) completes the x_g determination from (12). The quality of this reconstruction for J/Ψ events is shown in fig. 5 where we plot x_g vs. x_g^{rec} (5a and b) and the distribution in the resolution $(x_g - x_g^{rec})/x_g$ (5c). We find that x_g can determined with good quality (FWHM= 0.12, fig. 5c) over the whole range

$$3 \times 10^{-5} < x_g < 1 \times 10^{-2} \qquad \text{at} \quad < \mu^2 > \sim 25\,\text{GeV}^2 \tag{15}$$

where the average value of $\mu \equiv \sqrt{\hat{s}}$ is rather independent of x_g.

Having reconstructed x_g we now proceed to determine the input gluon density. It is related to the measured distribution $d\sigma/dx_g$ via

$$g(x_g, \mu^2(x_g)) = \frac{d\sigma(x_g)/dx_g|_{exp}}{f(x_g)|_{MC}} \tag{16}$$

where $f(x_g)|_{MC} = 1/g(x_g)_{MC}\, d\sigma/dx_g|_{MC}$ is determined by the Monte Carlo program. We find that the systematic error is rather small. The reconstructed gluon density is shown in fig. 6. The statistical errors for an integrated luminosity of $50\,pb^{-1}$ (corresponding to $\sim$ 1 month running) are shown by the vertical error bars in fig. 6. We also show the gluon density as obtained from set B2 of Morfin-Tung. We find that our method can clearly discriminate between these different parametrizations and provides an excellent way of measuring the gluon density in ep collisions at LEP/LHC energies.

3 $c\bar{c}$ and $b\bar{b}$ analysis

The signatures we want to exploit to identify the "signal" reactions (1) are based on the semileptonic decays of the heavy quarks. Specifically, we require two opposite sign leptons, electrons or muons. For our analysis we generate complete event samples using a modified version of the event generator AROMA both for signal events (1) as well as for the other processes discussed below. AROMA[8] contains gluon emission from the $Q\bar{Q}'$ system in a parton cascade approach and hadronization according to the LUND string model and heavy flavour decay. We assume a beam pipe of opening angle of 100 mrad. We require a minimal total transverse energy in the calorimeter for triggering purpose. In order to be measurable we demand a minimal transverse momentum p_T for the two leptons. Thus we have:

$$\sum E_T > 10\ \text{GeV} \quad , \quad p_T(l^{\pm}) > 1\,\text{GeV} \quad , \quad \theta_{\text{beam}} = 100\,\text{mrad}\,. \qquad (17)$$

After these cuts we obtain the following cross sections at $\sqrt{s} = 1.265\,\text{TeV}$ (including the K-factors stated in chapter 1):

$$\sigma(c\bar{c}) = 1.5\,\text{nb} \quad , \quad \sigma(b\bar{b}) = 1.0\,\text{nb}\,. \qquad (18)$$

Corrections given by the hadronic component of the photon to (1) are important. For open heavy quark production the leading order contributions are $q\bar{q} \to Q\bar{Q}$ and $gg \to Q\bar{Q}$. We studied the question of y reconstruction in detail following the lines in the previous section. We reconstruct y from all stable particles outside the beam pipe using (9). Again we find that y can very well be reconstructed for the signal events (1). For resolved photon events the photon remnants are mostly lost into the beam pipe. Thus (9) yields y_p (10) to a rather good accuracy. Since the gluon initiated subprocess is by far dominating the resolved photon contribution will depend on the gluon density in the proton in just the same way as the direct channel does. Both samples could therefore be added. Let us emphasize that the results depend on details of the fragmentation of the photon spectator jet and the detector acceptance. More work is needed to settle the question of reconstructing the kinematics of resolved photon processes. For the subsequent analysis we omit the resolved contribution, assuming that it either behaves like signal events or can be discriminated via the photon remnants by suitable detectors in the backward direction.

Background events come from the production of light quark events with subsequent decays into leptons. As was shown in [15] already weak isolation requirements on the leptons kill practically all background events without significant losses of charm and bottom events. The background is also reduced to a negligible level by a cut on the invariant mass of the lepton pair. For background events $m(l^+l^-)$ peaks at small values, whereas signal events have a rather wide distribution. We thus imposed the cut $m(l^+l^-) > 1\,\text{GeV}$. A discrimination of charm and bottom events is not necessary. The cut (17) on $\sum E_T$ implies a rather strong cut on $\hat{s}$ (remember $\sqrt{\hat{s}_{min}} = 2m_Q$). In fact, the average $\sqrt{\hat{s}}$ is about 11 GeV in the smallest x_g-bin and rises to about 100 GeV at large x_g. Hence we can combine charm and bottom events.

In open heavy quark production it is more difficult to find observables which can be measured experimentally and are related to x_g. We did not find a satisfying way to measure $\hat{s}$. Among the variables we tried are $\sum E_T$, the total visible energy, the invariant mass of the lepton pair, and transverse energies combined with polar angle information obtained from the leptons. In [15] two of us proposed another way to determine x_g which is based on the rapidity $\hat{y}$ of the partonic system:

$$\hat{y} = \frac{1}{2} \ln \left[\frac{y\, E_e}{E_p(x_g - Q^2/s)} \right] \qquad (19)$$

The crucial point is now that $\hat{y}$ can well be approximated by the rapidity of the lepton pair. This is documented in fig. 7 where we plot y_{ll} vs. $\hat{y}$. As in the case of J/Ψ production we approximate Q^2 by zero. We reject events at high Q^2 by requiring that the scattered electron cannot be identified. Combining the y and $\hat{y}$ measurements we find the following kinematic range explorable in heavy quark production at LEP/LHC:

$$6.3 \times 10^{-5} < x_g < 0.05 \qquad \text{at} \qquad < \mu^2 > \approx x_g^{0.46}\, 10^4\,\text{GeV}^2 \qquad (20)$$

The kinematic range is limited by statistics, the range in $\hat{y}$, and the total transverse energy cut in (17). Note that the average scale increases with x_g. The quality of the x_g determination is only slightly worse than in the J/Ψ case. In fig. 8 we show the probability that $x_g = 10^{-3}$ is reconstructed as x_g^{rec}. We find that the distribution peaks at the input value.

Systematic errors on event number enter since the measured values, x_g^{rec}, differ from the true x_g values and the number of events seen $\mathcal{L}\,\Delta x_g\, d\sigma/dx_g(x_g)|_{exp}$ in a bin of width Δx_g will differ from the true number $\mathcal{L}\,\Delta x_g\, d\sigma/dx_g(x_g)|_{MC}$ (at a given integrated luminosity $\mathcal{L}$). We use the Monte Carlo to correct for these efects using (16). The systematic error on this correction was estimated by varying the Monte Carlo functions $f|_{MC}$ using different gluon distribution functions. We adopted the bin sizes Δx_g at the edges of $d\sigma/dx_g$ such that migrations out and into the bins remained small. The result of this is shown in fig. 9 where the error bars indicate the systematical and statistical uncertainties. In fact, the statistical errors are very small. To guide the eye we have included the input density evaluated at the average $< \mu > = < \mu(x_g) >$. We also show the gluon density as obtained from set B2 of Morfin-Tung. We see that we can expect to discriminate between different

gluon distributions very well. The discrimination power clearly improves for lower x values.

Since the rates for open heavy flavour production are so large, we tried to reconstruct the gluon density at two different values of the scale argument. As stated above, the measurement of $\hat{s}$ is poor. Also the reconstruction from (19) is not particularly useful. We thus impose a larger cut in $\sum E_T$, $\sum E_T > 35\,\mathrm{GeV}$. This increases the average μ^2 by about a factor four to five almost uniformly over the entire x_g range. The reconstructed gluon density for this sample with $\sum E_T > 35\,\mathrm{GeV}$ is shown in fig. 10 together with the input gluon density at the corresponding average values of $\mu = \mu(x_g)$. Even when applying such a high cut in $\sum E_T$ the statistical error remains small. Also the systematical error is small enough in order to allow a discrimination against the gluon density evaluated at the lower scale values corresponding to the sample with $\sum E_T > 10\,\mathrm{GeV}$. We thus conclude that it seems possible to measure the gluon density in open heavy quark production over the wide range specified in (20) at an average scale and in an somewhat reduced range even as a function of the scale:

$$\begin{aligned} 400 < \mu^2 < 1600\,\mathrm{GeV}^2 \quad &\text{at} \quad x_g = 0.001 \\ 2300 < \mu^2 < 7800\,\mathrm{GeV}^2 \quad &\text{at} \quad x_g = 0.020\,. \end{aligned} \tag{21}$$

4 Discussion and Summary

In this work we investigated the prospects of extracting the gluon density from open and hidden heavy quark production in ep collisions at LEP/LHC energies. The analysis is based on complete (signal and background) events and, in the case of J/Ψ, it includes a full detector simulation. The reconstruction of the event kinematics is carefully outlined, in particular uncertainties due to unsufficient known fragmentation properties of the proton remanats and photon spectator jet are discussed. Higher order corrections on the event topology are approximately taken into account by multiple gluon radiation in a parton cascade approach. Only information obtainable from a main detector is used. In a previous study on gluon extraction from J/Ψ events at HERA[4] the information on the scattered electron coming from a luminosity monitor measurement has been used. This is not done here since it is not clear whether such a device will work with the high rates expected at LEP/LHC. Furthermore it was found that with the main detector a much larger range in x is accessible, including the range reachable via the luminosity measurement.

The outcome is that one will obtain measurements of $d\sigma/dx_g$ which are accurate enough to extract the gluon distribution at small-x, and hence to distinguish between different parametrizations, even if LEP/LHC is run at 10% of the design integrated luminosity ($1\,\mathrm{fb}^{-1}$ per year) only. The succesful reconstruction of the glue from open heavy quark production is demonstrated here for the first time. We estimate the explorable ranges to be $3 \times 10^{-5} < x_g < 1 \times 10^{-2}$ at an average scale of $\mu^2 \approx 25\,\mathrm{GeV}^2$ for J/Ψ production, and $6.3 \times 10^{-5} < x_g < 5 \times 10^{-2}$ at an average scale of $\mu^2 \approx \sqrt{x_g}\,10^4\,\mathrm{GeV}^2$ for $c\bar{c}$ and $b\bar{b}$ production. The larger lower

limit of x_g for the latter case arises from the fact that harder cuts are necessary to trigger and identify open heavy quark events. Though the distribution in the invariant mass $\sqrt{\hat{s}}$ of the $Q\bar{Q}$ subsystem is steeply falling, events at high $\hat{s}$ will copiously be produced due to the large rates expected at LEP/LHC. Cuts in the total transverse energy define samples with different average values of the scale argument μ of the gluon density which we took to be $\mu = \sqrt{\hat{s}}$. Hence we expect the evolution of the gluon density with μ to be observable in open heavy quark production at LEP/LHC. The explorable range is estimated in (21).

Systematical uncertainties arise due to unknown higher order corrections. The strong scale dependence of the cross sections as well as the expected large K factors indicate the importance of such corrections. The full one-loop corrections to the photoproduction of heavy flavours are known for the one heavy quark inclusive distributions[7]. For the purpose of extracting the gluon density along the lines discussed here it is necessary to have available the analogous calculation of the di-heavy quarks invariant mass and rapidity distributions, or even better the fully differential cross section evaluated at next-to-leading-order (NLO). Such a calculation needs in addition a correct treatment of the bound state system to that order for J/Ψ events. Consistent NLO calculations require the inclusion of the resolved photon processes with appropriate caveats of double counting the collinear contributions. It is clear that our results have to be interpreted as the extraction of the leading order gluon density. A determination accurate to NLO would require the implemention of the above mentioned corrections. Let us add that at the high cms energies at LEP/LHC a description based on fixed order QCD calculations (even with the inclusion of the NLO corrections) might not be adequate due to large logarithmic terms[16] like m_{TQ}^2/s where $m_{TQ}^2 = p_{TQ}^2 + m_Q^2$. It would be very useful to compare with an alternative description where such terms are resummed to all orders.

With the very small values of x reachable at LEP/LHC one will likely enter a region where the standard QCD evolution à la Dokshitser, Gribov, Lipatov, Altarelli, and Parisi[17] ceases to be valid. Screening corrections are expected to become sizeable[18]. The analyses presented here use the conventional approach[17] in the evolution of the parton densities. New calculations of cross sections and differential distributions based on the improved evolution scenario are necessary and eagerly awaited.

All of the above results are obtained assuming that LEP/LHC is run solely at a fixed cms energy ($\sqrt{s} = 1.26\,\mathrm{TeV}$). Data at different cms energies are highly desirable to check the theoretical predictions and to put the description of the events on a firmer basis. Changes of $\sqrt{s}$ will also move the accessible x_g ranges accordingly. The value of the scale $\mu = \sqrt{\hat{s}}$ is not expected to be affected for J/Ψ production since the rate is relatively low and thus the steeply falling $\hat{s}$-distribution is probed essentially at $\hat{s}_0 = (m_\Psi + 2p_T)^2 \approx 25\,\mathrm{GeV}^2$, roughly independent of $\sqrt{s}$. In the case of open heavy flavour production, however, there is strong correlation between the average scale and the cms energy. Here runs of LEP/LHC at various cms energies would clearly allow measurements of the gluon density over a wide $\{x, Q^2\}$ region.

References

[1] G. Ingelman, *Structure function measurements at LEP/LHC*, to be published in the Proceedings of the ECFA Workshop on LHC, Aachen, FRG (1990).

[2] J. Blümlein, *QCD tests at LEP/LHC*, to be published in the Proceedings of the ECFA Workshop on LHC, Aachen, FRG (1990).

[3] N. Magnussen and G. A. Schuler, *Extracting the gluon density from the longitudinal structure function*, to be published in the Proceedings of the ECFA Workshop on LHC, Aachen, FRG (1990).

[4] S.M. Tkaczyk, W.J. Stirling and D.H. Saxon, in Proceedings of the HERA workshop, DESY, Hamburg 1987.

[5] G. D'Agostini and D. Monaldi, DESY preprint, DESY 90-015 (1990).

[6] J.G. Morfin and Wu-Ki Tung, Fermilab-Pub-90/74 (1990).

[7] R. K. Ellis and P. Nason, Nucl. Phys. B312 (1989) 551;
W. Beenakker, W. L. van Neerven, R. Meng, G. A. Schuler and J. Smith, DESY preprint DESY 90-064, Nuclear Physics B in press;
G. A. Schuler, DESY-89-019 and in Proceedings of the 5^{th} workshop of the INFN Eloisatron Project, Erice, Italy 1988, Editor: A. Ali.

[8] G. Ingelman and G. A. Schuler, Z. Phys. C40 (1988) 299.

[9] R.Baier and R.Rückl, Nucl. Phys. B201 (1982) 1.

[10] Z. Kunszt and W.J. Stirling, Phys. Lett. B217 (1989) 563;
R.S. Fletcher, F.Halzen and R.W.Robinett, Phys. Lett. B225 (1989) 1.

[11] C. Albajar et al., Phys. Lett. B200 (1988) 381;
E.W.N.Glover, F.Halzen and A.D.Martin, Phys. Lett. B185 (1987) 441;
E.W.N.Glover, A.D.Martin and W.J. Stirling, Z. Phys. C38 (1988) 473.

[12] B. van Eijk and R.Kinnunen, Z. Phys. C41 (1988) 489.

[13] Technical Proposal for the H1 detector, H1 Collaboration (1986).

[14] K.J. Abraham, Nikhef Preprint 91-02.

[15] G. A. Schuler and J. F. de Trocóniz, DESY preprint in preparation.

[16] S. Catani, M. Ciafaloni and F. Hautmann, Phys. Lett. B242 (1990) 97.

[17] Yu.L..Dokshitser, *Sov.Phys.JETP* 46, 641(1977);
V.N.Gribov and L.N.Lipatov, *Sov.Journ.Nucl.Phys.* 15, 438 and 675 (1972);
G.Altarelli and G.Parisi, *Nucl.Phys.* 126, 297(1977).

[18] *Proceedings of the Small-x Workshop*, held at DESY, May 1990 (to be published in *Nucl.Physics*, ed.A.Ali and J.Bartels).

Figure captions

Figure 1 p_T distributions of the various J/Ψ production mechanisms: direct production (solid line, eq. (2)), resolved photon contributions (dashed line, eq. (4)), and b decays (dashed-dotted line, eq. (3)). The curves show the Monte Carlo p_T^{Ψ} distributions where no cut was applied.

Figure 2 Monte Carlo distributions in the polar angle in the Lab system, $d\sigma/d\cos\theta$, of J/Ψ's produced via the direct process (solid line) and the hadronic component of the photon (dashed line). Only a cut $p_T^{\Psi} > 1\,\mathrm{GeV}$ was applied.

Figure 3 Distributions in the variable z (eq. 6) for J/Ψ's events after demanding that they can be reconstructed in the tracking system and after a cut $p_T^{\Psi} > 1\,\mathrm{GeV}$. Monte Carlo results for the direct process as solid line, for the hadronic component of the photon in dashes. Distributions in the reconstructed z_{rec} (eq. 8) in dash-dots for the direct channel and in dots for the resolved photon one.

Figure 4 The correlation y vs. the reconstructed y_{rec} (eqs. 7 and 9) for J/Ψ production via the direct process (a) and the hadronic component of the photon (b). Correlation y_p vs. y_{rec} (eq. 10) in Fig. 4c.

Figure 5 The correlation x_g vs. the reconstructed x_g^{rec} for J/Ψ's production via the direct process (a) and the hadronic component of the photon (b). The resolution of the reconstructed x_g^{rec} (c).

Figure 6 The reconstructed gluon density from J/Ψ production with statistical error bars corresponding to an integrated luminosity of $50\,pb^{-1}$ for set B1 and $20\,pb^{-1}$ for set B2 (upper points). Also shown are the input gluon densities set B1 and B2 (dashed line) of ref.[6].

Figure 7 The correlation y_{ll} vs. $\hat{y}$ (eq. 19) for open heavy quark production.

Figure 8 Probability distribution that the true $x_g = 10^{-3}$ is reconstructed as x_g^{rec} for open heavy quark production.

Figure 9 The reconstructed gluon density for open heavy quark production including systematic and statistical errors. Also shown are the input gluon density (set B1 of ref.[6]) and the gluon density B2 of ref.[6] both evaluated at the average scale $< \mu^2 >=< \hat{s} > (x_g)$.

Figure 10 The reconstructed gluon density for open heavy quark production including systematic and statistical errors for the sample with $\sum E_T > 10\,\mathrm{GeV}$ and for the sample with increased cut $\sum E_T > 35\,\mathrm{GeV}$ (upper points). Also shown is the input gluon density (set B1 of ref.[6]) evaluated at the respective average scales $< \mu^2 >=< \hat{s} > (x_g)$ corresponding to the two samples $\sum E_T > 10\,\mathrm{GeV}$ and $\sum E_T > 35\,\mathrm{GeV}$.

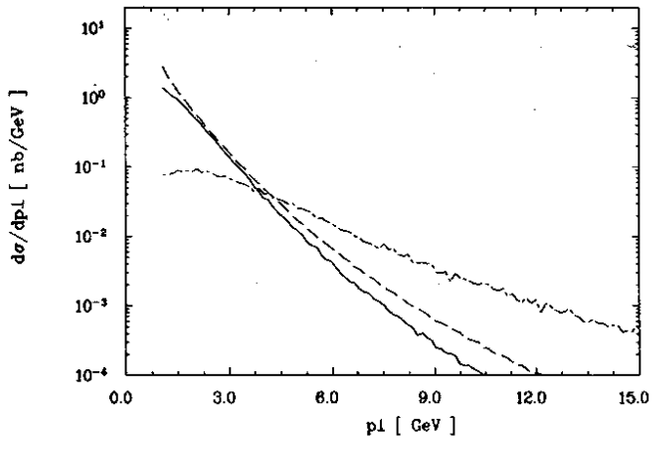

Fig. 1

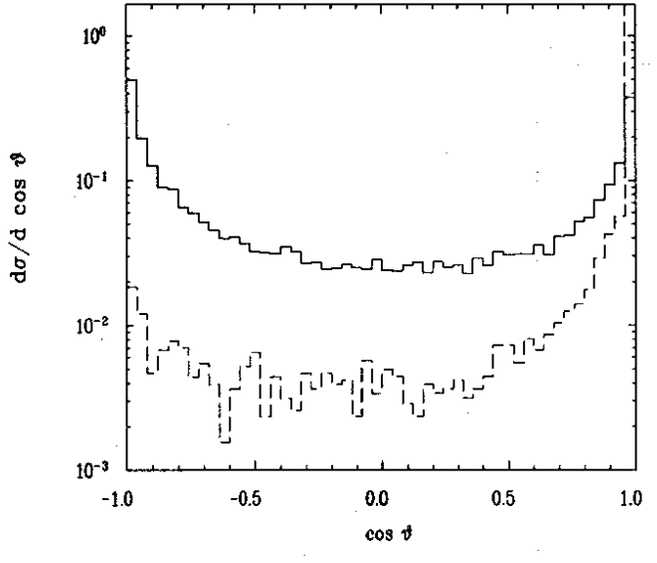

Fig. 2

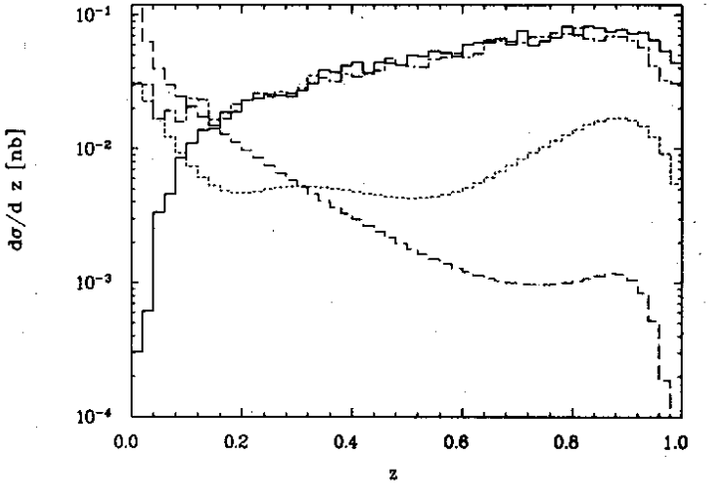

Fig. 3

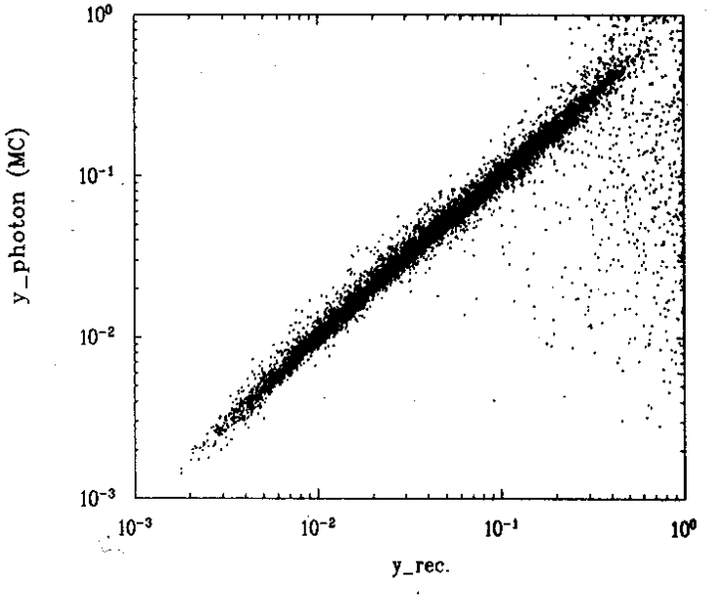

Fig. 4 a

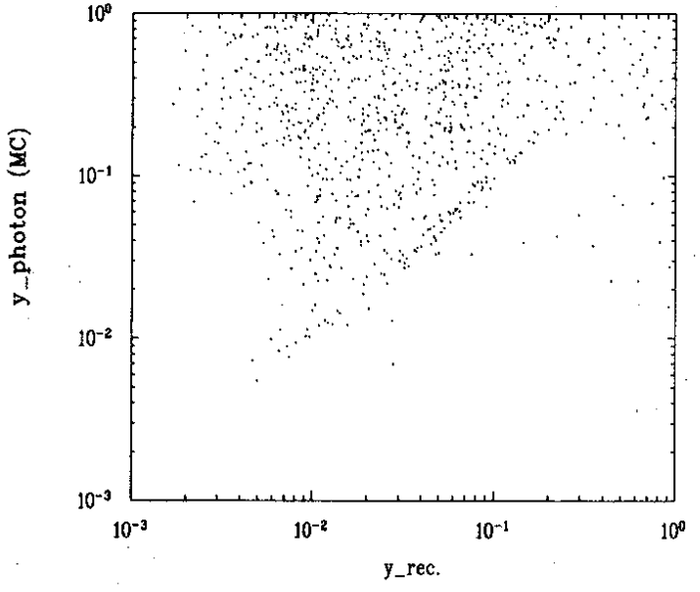

Fig. 4 b

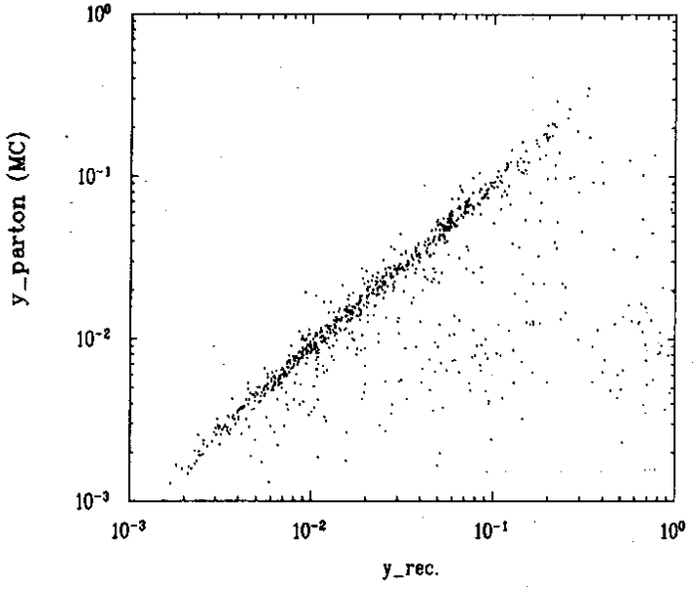

Fig. 4 c

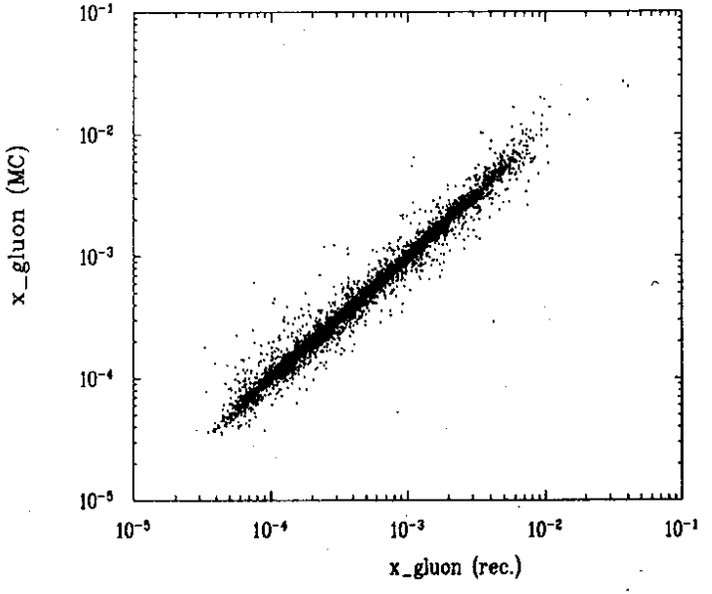

Fig. 5 a

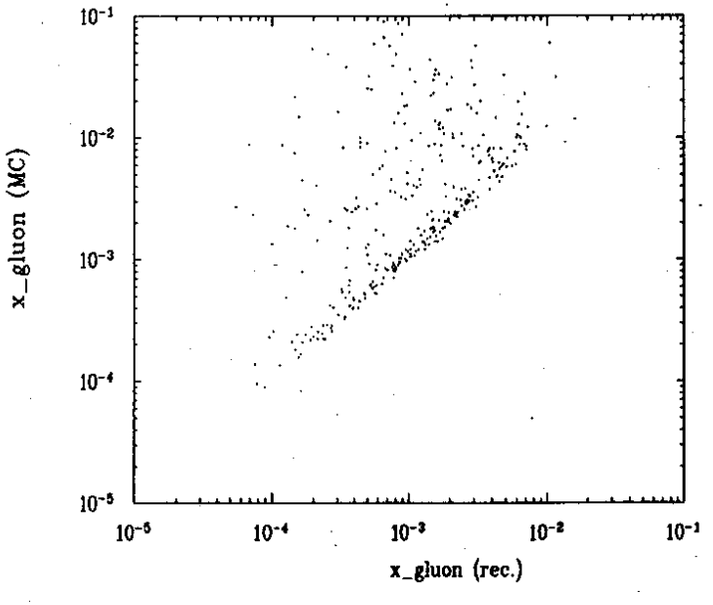

Fig. 5 b

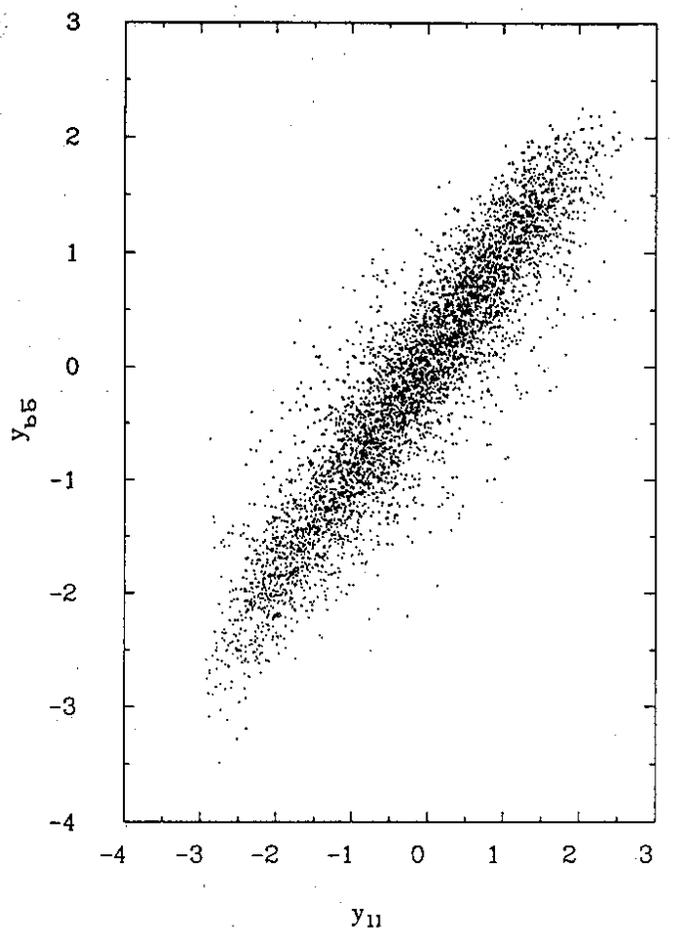

Fig 7

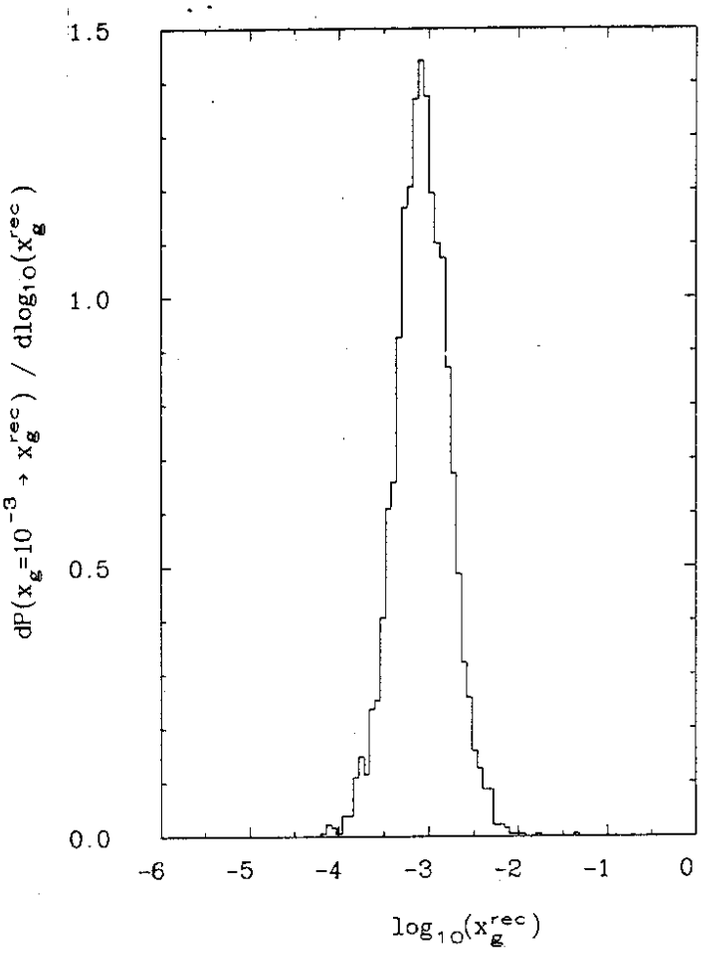

Fig 8

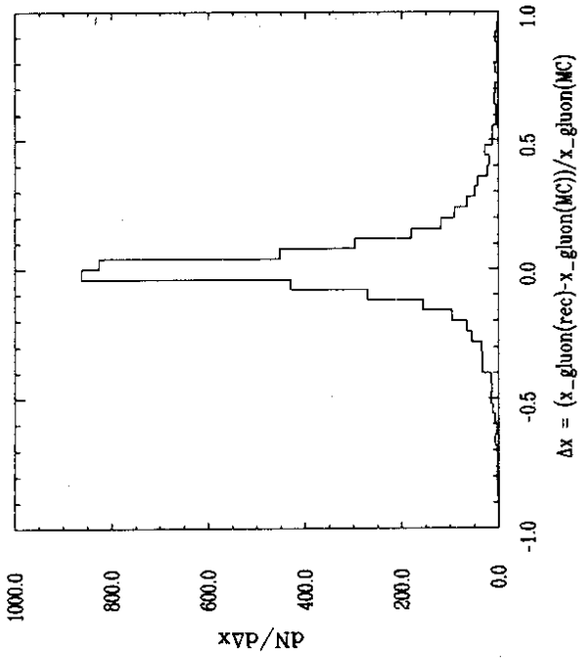

Fig. 5 c

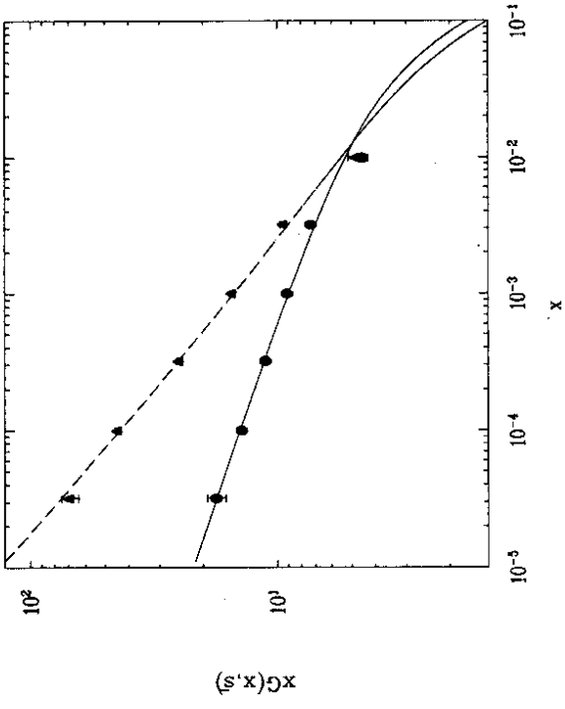

Fig. 6

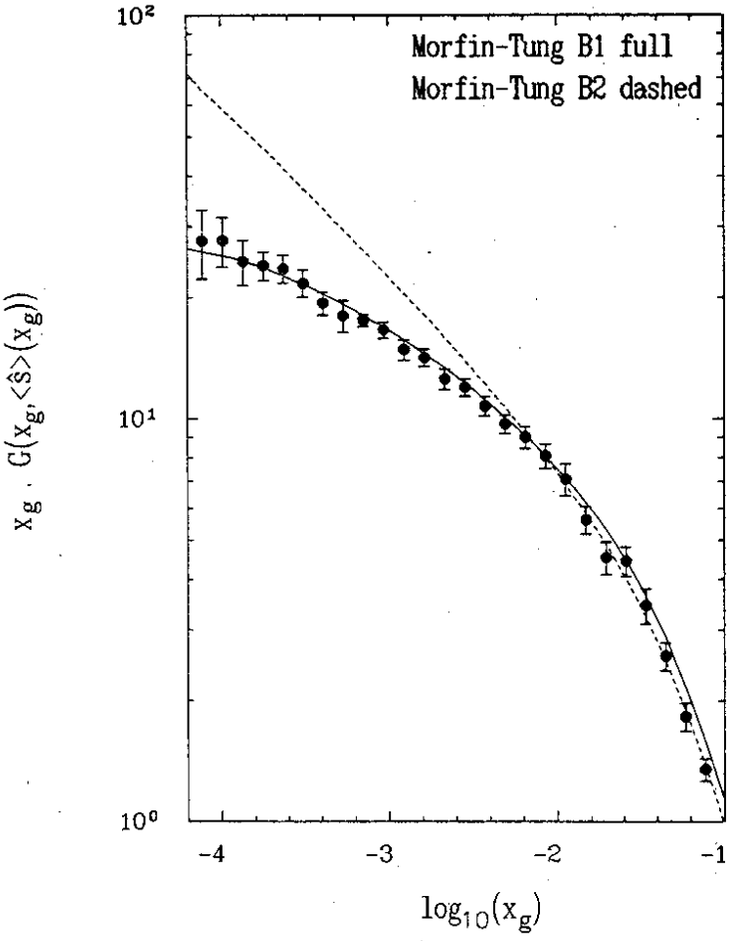
Morfin-Tung B1 full
Morfin-Tung B2 dashed
10^2
10^1
10^0
-4
-3
-2
-1
$x_g \cdot G(x_g, \langle \hat{s} \rangle (x_g))$
$\log_{10}(x_g)$

Fig 9

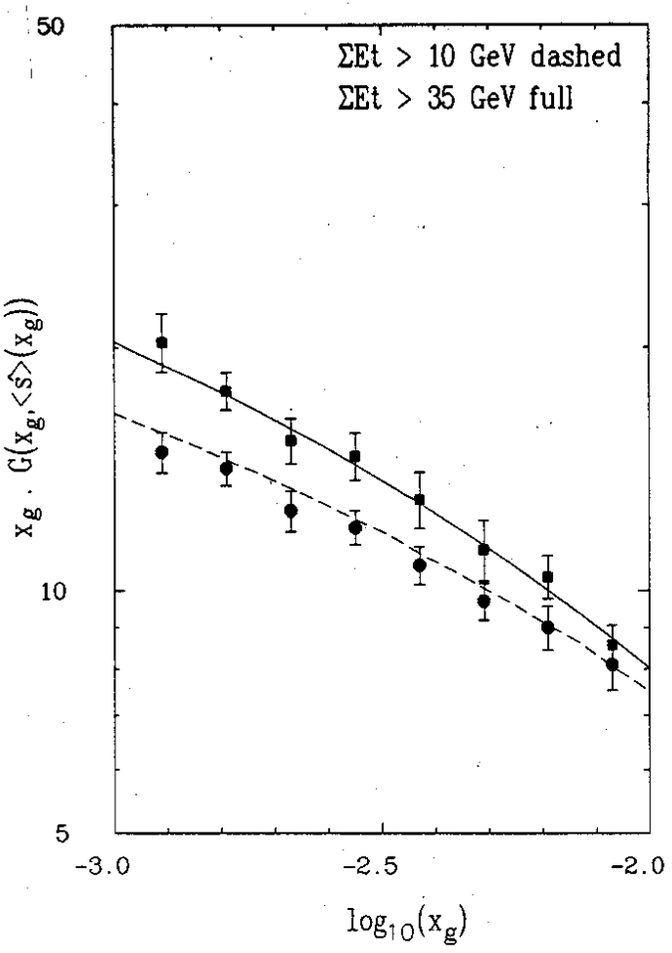
ΣEt > 10 GeV dashed
ΣEt > 35 GeV full
50
10
5
-3.0
-2.5
-2.0
$x_g \cdot G(x_g, \langle \hat{s} \rangle (x_g))$
$\log_{10}(x_g)$

Fig 10